Routes to complex dynamics in a ring of unidirectionally coupled systems

P. Perlikowski[1,2], S. Yanchuk[1], M. Wolfrum[3], A. Stefanski[2], P. Mosiolek[4] and T. Kapitaniak[2]
[1] *Institute of Mathematics, Humboldt University of Berlin, Unter den Linden 6, 10099 Berlin, Germany*
[2] *Division of Dynamics, Technical University of Lodz, Stefanowskiego 1/15, 90-924 Lodz, Poland*
[3] *Weierstrass Institute for Applied Analysis and Stochastics, Mohrenstrasse 39, 10117 Berlin, Germany and*
[4] *Institute of Automatic Control, Technical University of Lodz, Stefanowskiego 18/22, 90-924 Lodz, Poland**

We study the dynamics of a ring of unidirectionally coupled autonomous Duffing oscillators. Starting from a situation where the individual oscillator without coupling has only trivial equilibrium dynamics, the coupling induces complicated transitions to periodic, quasiperiodic, chaotic, and hyperchaotic behavior. We study these transitions in detail for small and large numbers of oscillators. Particular attention is paid to the role of unstable periodic solutions for the appearance of chaotic rotating waves, spatiotemporal structures and the Eckhaus effect for a large number of oscillators. Our analytical and numerical results are confirmed by a simple experiment based on the electronic implementation of coupled Duffing oscillators.

I. INTRODUCTION

Theoretical and experimental investigations have shown that coupled systems, in particular large coupled systems, have a great potential in a large amount of application areas ranging from physics and engineering to economy and biology. In this paper we show that a ring of unidirectionally coupled Duffing oscillators demonstrates complex dynamical behavior. We observe periodic, quasiperiodic, chaotic, and hyperchaotic attractors. In the chaotic regime, chaotic rotating waves are identified. For a large number of oscillators we observe the emergence of spatiotemporal structures and the appearance of the Eckhaus scenario. We partially verify our results in a simple electronic experiment.

Recently, one can observe a growing interest in the studies of the networks of coupled oscillators [1]. The knowledge of the dynamical behavior of such systems can contribute to the understanding of fundamental dynamical features of physical, biological, engineering or economical coupled systems [2, 3]. The most important question is how the specific properties of the individual behavior and the coupling architecture can give rise to different types of collective behavior [4]. The other problem, which is discussed here, is connected with the structure of the attractors in higher dimensional phase space and, in particular, with the occurrence of the hyperchaotic attractors. If a map is at least two-dimensional or a flow is at least four-dimensional, its evolution can take place on a hyperchaotic attractor. Such attractors are characterized by at least two positive Lyapunov exponents for typical trajectories on them. The first example of such a system with hyperchaotic attractor was presented by Rössler [5] for a chemical reaction model. Later, hyperchaotic attractors have been found in electronic circuits and other chemical reactions [6, 7]. In the works [8, 9] it was shown that by a weakly coupling of N chaotic systems it is possible to obtain a hyperchaotic attractor with N positive Lyapunov exponents. The transition from chaos to hyperchaos has been studied in [10–12]. It was shown that at this transition the attractor's dimension and the second Lyapunov exponent grow continuously. The role of the unstable periodic solutions in this transition has been discussed in [13–15].

In this paper we present a mechanism that leads to a transition from periodic to chaotic and hyperchaotic behavior in a ring of unidirectionally coupled autonomous Duffing oscillators only by increasing the coupling strength. This is done by analyzing the destabilization of the steady state, numerical simulation of bifurcating attractors and calculation of the full spectrum of Lyapunov exponents. We give evidence that the coupling symmetry of the considered system implies a phase relation that is preserved for chaotic behavior and creates chaotic rotating waves [16–18]. For a large number of oscillators we observe the coexistence of several periodic solution branches with a stability boundary that can be interpreted in terms of the classical Eckhaus scenario as a sideband instability within a family of solutions with different periods in space and time [19–25]. We calculate the symmetric unstable periodic orbits (UPO), identify their role in the skeletons of the chaotic and hyperchaotic attractors, and point out their importance for the development of spatio-temporal structures. Finally, we report on the electronic implementation of a ring of three Duffing oscillators and show experimental results that partially confirm the existence of the chaotic rotating waves.

This paper is organized as follows: In Sec. II we introduce our system. The study of the stability of the equilibrium state of a ring of N oscillators is presented in Sec. III. Section IV describes the dynamics of a ring of three coupled oscillators. In this section we present both numerical and experimental results. In Sec. V we study the appearance of a chaotic rotating waves. The dynamics of a large ring of 400 oscillators is investigated in Sec. VI where we observe the Eckhaus effect and the creation of complex spatio-temporal structures. Finally,

*Electronic address: `przemyslaw.perlikowski@p.lodz.pl`

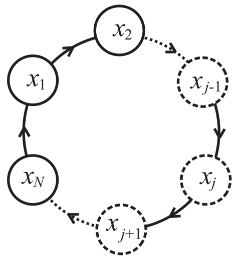

Figure 1: Ring of unidirectionally coupled oscillators.

we give conclusions in Sec. VII.

II. THE MODEL

We consider the ring of unidirectionally coupled oscillators shown in Fig. 1. As a node system we take the autonomous Duffing oscillator described by the following second order ODE:

$$\ddot{v} + d\dot{v} + av + v^3 = 0, \tag{1}$$

where a and d are positive constants. In all numerical examples we use the fixed the parameter values $a = 0.1$ and $d = 0.3$. The system (1) is a single-well Duffing oscillator which has a single equilibrium point at $v = \dot{v} = 0$. Due to the presence of damping ($d > 0$) in the oscillator this equilibrium is an attractor for all initial conditions.

Introducing the new coordinates $x = v$, $y = \dot{v}$ in Eq. (1) the dynamics of the ring of oscillators shown in Fig. 1 can be described by the following system:

$$\begin{aligned} \dot{x_j} &= y_j, \\ \dot{y_j} &= -dy_j - ax_j - x_j^3 + k\left(x_{j-1} - x_j\right), \end{aligned} \tag{2}$$

where k is a linear coupling coefficient and $j = 1, \ldots, N$ is considered modulo N. This type of unidirectional coupling appears in different applications, e.g. in reactive flows [26, 27], motions of active Brownian particles [28], etc.

More generally Eq. (2) with rotation-symmetric structure of the coupling can be rewritten in the following form:

$$\dot{z}_j = Az_j + B(z_j) + Hz_{j-1}, \tag{3}$$

where A is the Jacobian of the node system, $B(z_j)$ represents non-linear terms and the matrix H takes care for the coupling to the $(j-1)$th neighbor. For the system (2) we obtain

$$A = \begin{bmatrix} 0 & 1 \\ -(a+k) & d \end{bmatrix},\ B(z_j) = \begin{bmatrix} 0 & 0 \\ -x_j^3 & 0 \end{bmatrix},\ H = \begin{bmatrix} 0 & 0 \\ k & 0 \end{bmatrix}, \tag{4}$$

where $z_j = (x_j, y_j)^{\mathrm{T}}$.

The entire coupled system can be described in the matrix form:

$$\dot{\mathbf{z}} = (\mathbf{I} \otimes A)\mathbf{z} + \mathbf{B}(\mathbf{z}) + (\mathbf{G} \otimes H)\,\mathbf{z}, \tag{5}$$

where $\mathbf{z} = (z_1, \ldots, z_N)^{\mathrm{T}}$, $\mathbf{I}$ is the identity $N \times N$ matrix, and $\mathbf{B}(\mathbf{z}) = \operatorname{diag}(B(z_1), \ldots, B(z_N))$ are nonlinearities. $\mathbf{G}$ is the $N \times N$ connectivity matrix representing the topology of connections between the array nodes, and for the unidirectional ring structure we have

$$\mathbf{G} = \begin{bmatrix} 0 & 0 & 0 & \ldots & 1 \\ 1 & 0 & 0 & \ldots & 0 \\ . & . & . & . & . \\ 0 & \ldots & 1 & 0 & 0 \\ 0 & 0 & \ldots & 1 & 0 \end{bmatrix}. \tag{6}$$

Eq. (5) has a symmetric equilibrium point $\mathbf{z} = (0, \ldots, 0)^{\mathrm{T}}$.

III. STABILITY OF THE EQUILIBRIUM

In order to investigate the stability of the symmetric equilibrium point of the ring we linearize Eq. (5) in the neighborhood of $\mathbf{z} = (0, \ldots, 0)^{\mathrm{T}}$. The resulting variational equation has the following form:

$$\delta\dot{\mathbf{z}} = [\mathbf{I} \otimes A + \mathbf{G} \otimes H]\delta\mathbf{z}, \tag{7}$$

where $\delta\mathbf{z} = (\delta z_1, \ldots, \delta z_N)^{\mathrm{T}}$. After block diagonalization of the variational equation (7), there appear N independent systems [25, 29]

$$\dot{\xi}_j = (A + \gamma_j H)\,\xi_j, \quad j = 1, \ldots, N, \tag{8}$$

where ξ_j are variational coordinates and γ_j are the eigenvalues of the connectivity matrix $\mathbf{G}$, which can be calculated here easily as

$$\gamma_j = e^{i2\pi j/N} \tag{9}$$

where $j = 1, \ldots, N$. In this way, we reduce the stability problem for (7) to a family of characteristic equations

$$\chi(\lambda, j) := \det(\lambda I - A - \gamma_j H) = 0, \quad j = 1, \ldots, N \tag{10}$$

that determine the stability of different spatial patterns. When the number of oscillators N is large, we can replace the discrete family of network eigenvalues γ_j by the continuous family $e^{i\varphi}$, $\varphi \in (0, 2\pi)$ (cf. [25]) and obtain the equation

$$\chi(\lambda, \varphi) := \det\left(\lambda I - A - e^{i\varphi}H\right) = 0 \tag{11}$$

for the location of the eigenvalues for stationary state of system (7). For any number of coupled systems N the eigenvalues γ_j are located on closed curves (see Figs. 2a-c) given by solutions $\lambda(\varphi)$, $0 \leq \varphi \leq 2\pi$ of Eq. (11). The continuous curves $\lambda(\varphi)$ describe the spectrum for large N and are called asymptotic continuous spectrum (ACS) [25]. Indeed, for increasing N one can observe that ACS curves are more and more densely filled by eigenvalues.

The exact values of eigenvalues can be found from (10) as follows

$$\lambda_{1,2}(j) = -\frac{d}{2} \pm \sqrt{\left(\frac{d}{2}\right)^2 - a - k\left(1 - e^{i2\pi j/N}\right)} \quad (12)$$

and the corresponding formula for the ACS curves is

$$\lambda_{1,2}(\varphi) = -\frac{d}{2} \pm \sqrt{\left(\frac{d}{2}\right)^2 - a - k\left(1 - e^{i\varphi}\right)}. \quad (13)$$

The eigenvalues given by (12) determine the stability properties of the equilibrium for system (2). Figure 2 illustrates the eigenvalues and their dependence on the coupling parameter k. For increasing k, the stationary state loses its stability in a Hopf bifurcation. With an increasing number N of oscillators, the critical coupling strength (black vertical line in the right column) decreases. In the limit of $N \to \infty$ the critical value can be calculated as the touching point of the ACS with the imaginary axis. The corresponding value of φ determines the spatial pattern of the destabilizing mode. Note that there are further Hopf bifurcations, leading to multiple unstable periodic orbits. Their number N_{HB} is given for even N by $N_{HB} = \frac{N}{2} - 1$ and for odd N by $N_{HB} = \frac{N-1}{2}$. We will demonstrate later that primary branch of periodic orbits is stable, and the branches with frequency and spatial wave number close to the primary branch can also acquire stability, leading to scenario of multistability of periodic orbits. We will analyze this phenomenon in more detail in Sec. VI.

IV. NUMERICAL AND EXPERIMENTAL INVESTIGATION FOR $N = 3$

A. Destabilization route

In this section, we describe the destabilization mechanisms in the smallest interesting case of $N = 3$ Duffing oscillators. Indeed, for $N = 2$, the system has a decreasing energy for $d > 0$ and there is no destabilization induced by the coupling. We will first present our theoretical results and then compare them with an experiment on electrical circuits.

The first destabilizing Hopf bifurcation in the system occurs at $k = 0.238$ and creates a stable periodic solution (the bifurcation is supercritical). Further increasing coupling strength k leads to the appearance of quasiperiodic, chaotic, and hyperchaotic dynamics one after the other.

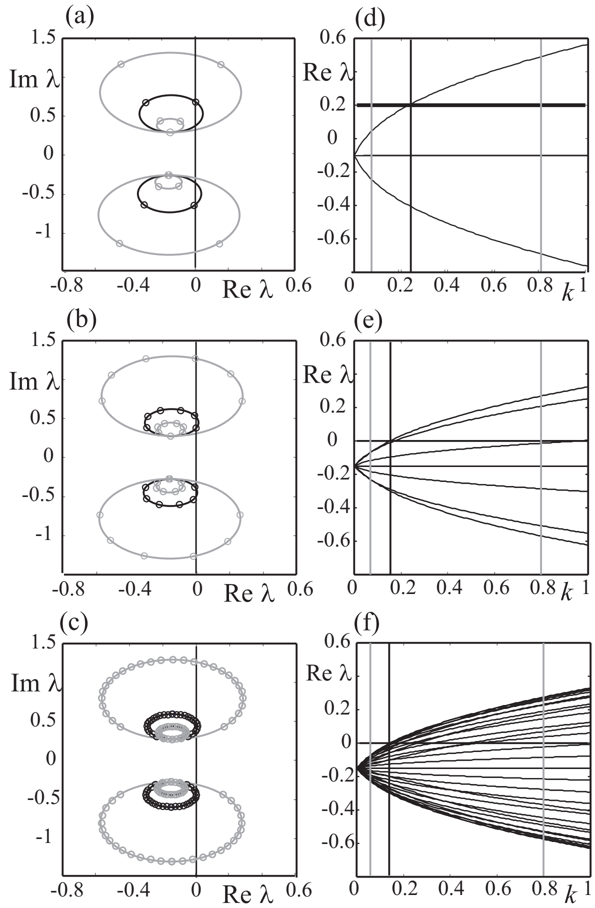

Figure 2: Left column: eigenvalues of the steady state and ACS in complex plane for three different values of k indicated by vertical lines on the right. Right column: real parts of eigenvalues versus coupling coefficient k. Number of oscillators: $N = 3$ (a), (b); $N = 7$ (c), (d); $N = 30$ (e), (f).

Fig. 4 illustrates different observed dynamical regimes and Fig. 3 gives the corresponding bifurcation diagram with respect to the control parameter k. Fig. 3(a) shows the bifurcation diagram for an arbitrarily chosen variable x_j. The corresponding plots of the four largest Lyapunov exponents [30, 31] are presented in Fig. 3(b). Figs 4(a-f) show Poincare maps for the different existing types of attractors.

The bifurcation diagram shows that the periodic solution (see Fig. 4(a)) appearing after the destabilization of the equilibrium via Hopf Bifurcation (HB) is stable up to the Neimark-Saker (NS) bifurcation at $k = 0.373$. Then it becomes unstable and stable a quasiperiodic solution (Fig. 4(b)) appears, which is characterized by two vanishing largest Lyapunov exponents. When the coupling strength reaches the value $k = 0.73$ one can observe a period doubling bifurcation of the torus (Fig. 4(c)) followed by an inverse period doubling (Fig. 4(d)) at $k = 1.4$. The doubling of torus periodicity is illustrated with the plots of time series in Fig. 4(h), where the doubling of the period is explicitly visible (compare Figs. 4(g) and 4(i)).

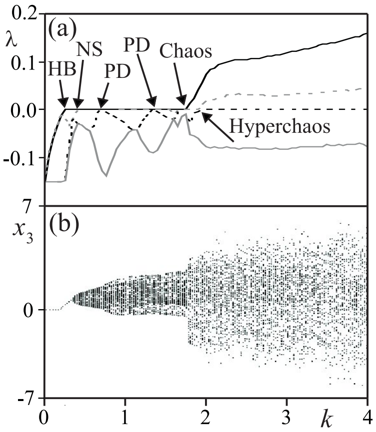

Figure 3: Four largest Lyapunov exponents (a) and bifurcation diagram (b) for the array of three coupled Duffing oscillators versus coupling coefficient k. Bifurcations occur for the following parameter values: Hopf bifurcation (HB) ($k = 0.238$), Neimark-Sacker bifurcation (NS) ($k = 0.373$), period-doubling bifurcations of a torus (PD) ($k = 0.73$ and $k = 1.4$), transition to chaos (Chaos) ($k = 1.79$), appearance of the second positive Lyapunov exponent (Hyperchaos) ($k = 1.9$). Parameters of the system $d = 0.3$ and $a = 0.1$.

For $k = 1.79$ the largest Lyapunov exponent becomes positive and the transition to chaos via torus breakdown takes place (Fig. 4(e)). Finally, for $k > 1.9$ the second largest Lyapunov exponent becomes positive and a hyperchaotic attractor shows up for larger coupling. The Poincare map of the hyperchaotic attractor is shown in Fig. 4(f).

In order to test experimentally our numerical results, we have performed a simple electrical experiment [32–34]. The electrical scheme of three coupled Duffing oscillators is shown in Fig. 5. Each oscillator is shown in a black frame and is build using two capacitors, six resistors and two multiplicators AD-633JN [35], which introduce nonlinearity. The characteristics of multiplicators is given by the following equation:

$$W = \frac{1}{V_c}(X_1 - X_2)(Y_1 - Y_2) + Z,$$

where X_1,X_2, Y_1, and Y_2 are input signals, W is the output signal, $V_c = 10$V and Z is a correction to the output signal. We measured the voltage at points V_{1-3} and δV_{1-3} which are related to x_{1-3} and y_{1-3} receptively. In order to set the initial conditions, we added an external impulse to the third system. The coupling is introduced through resistors R and potentiometer $R8$ which is a controlling device. In our experiment we used out of shelf elements: $C1 = C2 = 10uF$ $R1 = 1M\Omega$, $R2 = 333\Omega$, $R3 = 10M\Omega$, $R4 = R7 = 10k\Omega$, $R5 = R6 = 100k\Omega$, $R8 = \in [0\Omega, 44k\Omega]$, $R = 10k\Omega$, the accuracy is $\pm 1\%$.

The dynamics of the obtained electrical system is described by Eq. (2) where the dimensionless parameters are in the following relation with the parameters of the electrical circuit: $a = \frac{100R4}{R5}$, $d = \frac{1}{C1R1\omega_0}$, $k = \frac{R2}{R8}$, $x_{1-3} = \frac{V_{1-3}}{v_0}$, $y_{1-3} = \frac{\delta V_{1-3}}{v_0\omega_0}$, $\omega_0^2 = \frac{1}{100C1C2R4R7}$, and $v_0 = 1V$ is a scaling voltage [36]. The comparison of numerical simulations with experimental data is demonstrated in Figs. 6(a-l), where the numerically generated phase portraits (d-e, j-l) and their experimental counterparts (a-c, g-i) are shown. Each pair of phase portraits is related to the corresponding Poincare map and time diagram shown in Figs. 4(a-f), i.e. they have been obtained for corresponding values of the coupling parameter. A comparison of the results shows high qualitative agreement between the simulations and the experiment.

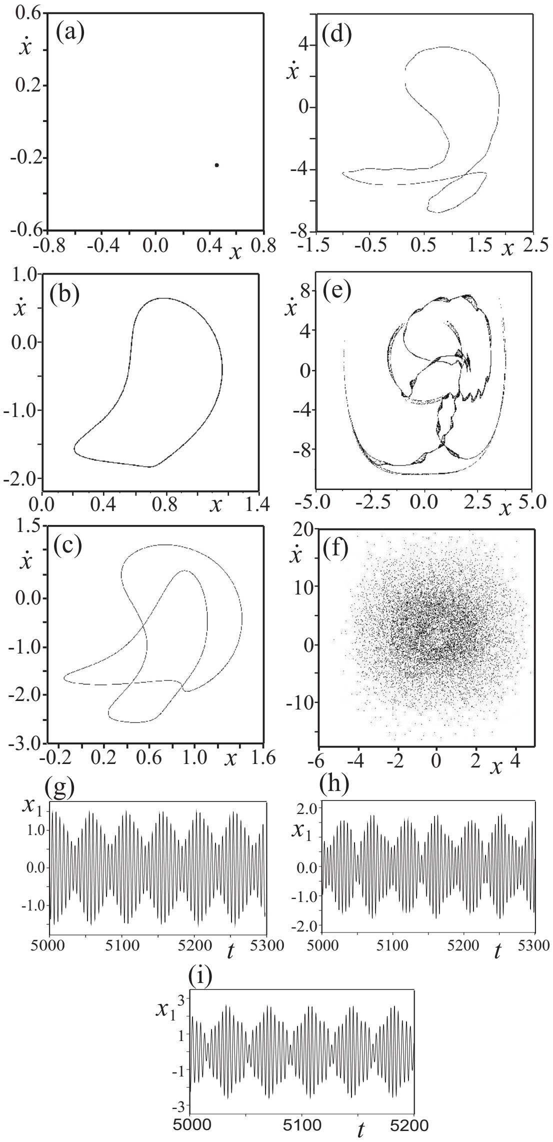

Figure 4: Three coupled Duffing oscillators: Poincare sections (a-f) and time traces (g-i) for the variable x_3; (a) periodic motion for $k = 0.3$, (b,g) quasiperiodic motion for $k = 0.67$, (c,h) torus after the period-doubling for $k = 0.77$, (d,i) torus after the inverse period doubling for $k = 1.77$, (e) chaotic attractor for $k = 1.8$, and (f) hyperchaos for $k = 2.1$. Parameters of the system $d = 0.3$ and $a = 0.1$.

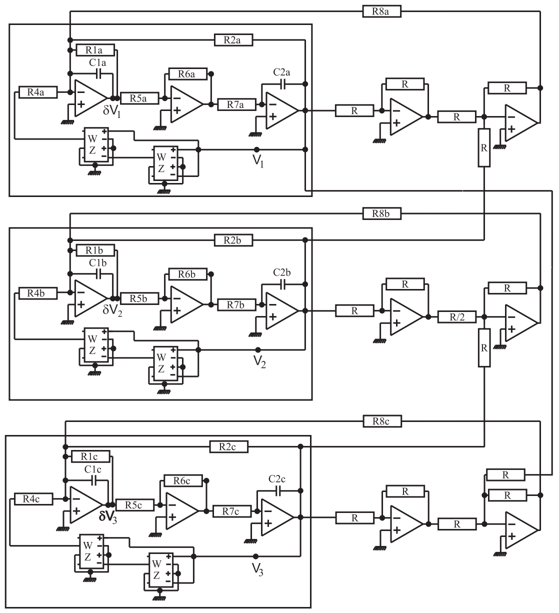

Figure 5: Electronic implementation of three unidirectionally coupled autonomous Duffing oscillators. More details are given in the text.

Slight differences are visible only in the shape but not in the type of corresponding attractors.

B. Periodic, quasi-periodic, and chaotic rotating waves

In this section we study the effects of the symmetry in the coupling structure on the dynamics. The invariance with respect to spatial rotation (index shift) of the system (2) implies the appearance of the solutions with prescribed spatio-temporal symmetry [37–39]. Such solutions in our case are time-periodic rotating waves, where all oscillators move along the same periodic orbit but with a fixed phase shift between neighboring nodes in the ring. One can show [25] that all periodic solutions, which appear after the Hopf bifurcations of the symmetric equilibrium of (2) (see Sec. III), possess this symmetry. In this section we demonstrate that these symmetry properties play an important role even for quasiperiodic and chaotic attractors appearing after the destabilization of the rotating waves. In particular, one can observe a phase-shifted chaotic or quasiperiodic synchronization.

Note that a complete synchronization [40], i.e. the full coincidence of phases and amplitudes of all coupled oscillators would lead in our case to vanishing coupling terms and consequently to the oscillation 'death' due to the internal damping (coefficient $d > 0$). On the other hand, in the case of unidirectionally coupled systems one can expect phase [41, 42] or generalized [43, 44] synchronization as well as the appearance of spatiotemporal structures [45–47]. In order to investigate the degree of the generalized synchronization, we decided to use the method based on computation of the localized sets [48]. The main idea of this method consists of the position detection of all oscillators in the time moments when the trajectory of some reference system (e.g. the state $(x_1, \dot{x}_1)$ of the first oscillator) is close to some point chosen arbitrary on the attractor. To this end, we define a small box D_1 in the plane $(x_1, \dot{x}_1)$. Then the set D_2 consists of all points $(x_2(t), \dot{x}_2(t))$ such that $(x_1(t), \dot{x}_1(t)) \in D_1$, i.e. determining the position of system 2 at the time moments when the first system is in the box D_1. Similarly the box D_3 is constructed. If the sets D_2 and D_3 for the second and the third systems are localized, one may speak about the existence of a generalized synchronization between the systems.

The corresponding localized sets for different attractors are shown in Fig. 7. For the periodic case (Fig 7(a)) the reference localized set D_1 (black) generates two corresponding localized sets D_2 (red) and D_3 (green), which are shifted by one third of the period along the same orbit. This fact indicates the presence of the periodic rotating wave. The same procedure is used now for the further dynamical states of the coupled system. Both, for quasi-periodic (Fig. 7(b)) and chaotic (Fig. 7(c)) attractors the corresponding sets are relatively well localized. The sets on the torus have approximately the same size as the reference D_1 (black) box. In the chaotic regime, the corresponding sets are visibly larger than the reference set.

In addition, in the case of torus one reference set D_1 generates two pairs D_2', D_2'' and D_3', D_3'' of localized sets, and in the case of chaotic attractor it generates two groups of four localized sets. For the parameter k values slightly larger than the Neimark-Sacker bifurcation point (NS in Fig. 3), the sets D_3' and D_3'' as well as D_2' and D_2'' approach each other and merge at the bifurcation point NS, where the periodic rotating wave appears. Therefore, the NS bifurcation can be regarded as a soft symmetry breaking bifurcation. At this bifurcation, with increasing of the control parameter k, the periodic rotating wave loses its stability and the bifurcating stable torus has no longer an exact spatio-temporal symmetry. As a result the sets D_2 and D_3 split into two pairs of localized sets D_2', D_2'' and D_3', D_3''.

The appearance of multiple localized sets can be also understood as follows. The reference box D_1 is in fact a projection of an unbounded cylindrical set in the 6-dimensional phase space of the coupled system $(x_1, \dot{x}_1, x_2, \dot{x}_2, x_3, \dot{x}_3)$ that intersects the attractor in the other localized sets. Hence, it is natural that for the torus we obtain two connected components in this cross-section. In Fig. 7(d) the localized set for a hyperchaotic attractor is shown. It is clearly visible that the points of the corresponding set are more uniformly distributed in large area on the attractor, which indicates higher degree of desynchronization.

In addition, the spatio-temporal symmetry of the system (2) implies that the periodic, quasiperiodic, and chaotic rotating waves appear [16–18, 49–51]. Indeed,

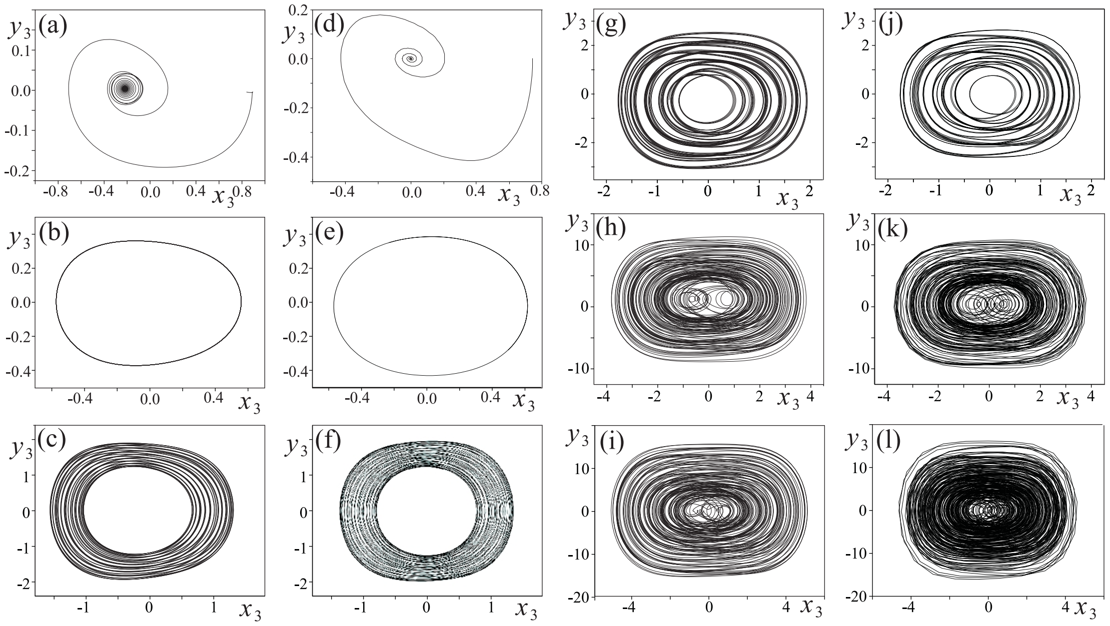

Figure 6: Comparison of experimental (a-c,g-i) and numerical results (d-f, j-l). Phase portraits are shown in projection onto the plane (x_3, y_3). Stable equilibrium (a,d), periodic solution (b,e), quasiperiodic solution or two-dimensional torus (c,f), quasiperiodic solution after the period-doubling (g,j), chaotic attractor (h,k), hyperchaotic attractor (i,l).

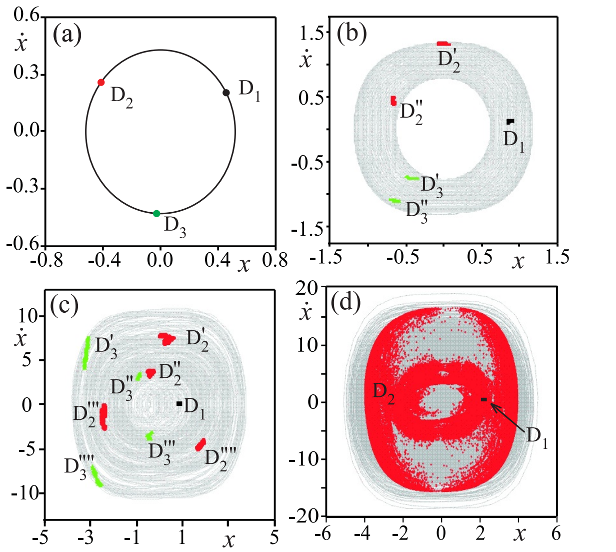

Figure 7: Localized sets with attractor in background for the array of three coupled oscillators. Parameters: $k = 0.3$ (a), $k = 0.5$ (b), $k = 1.8$ (c), $k = 2.1$ (d). Other parameters: $a = 0.1$ and $d = 0.3$.

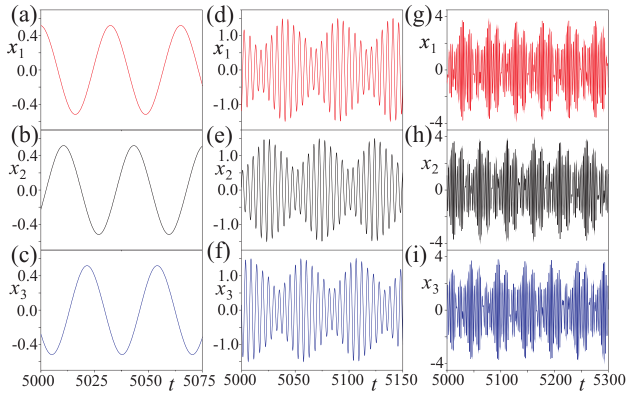

Figure 8: Comparison of time traces of different oscillators (in rows) in the ring of three electronic circuits shown in Fig. 5. (a-c) Periodic ($k = 0.3$), (d-f) quasi-periodic ($k = 0.67$) and (g-i) chaotic ($k = 1.8$) rotating waves. Other parameters: $a = 0.1$ and $d = 0.3$.

the quasiperiodic and chaotic attractors of our system possess the approximate spatiotemporal translation symmetry as it is shown in Figs. 8 and 9. Fig. 8 shows that the orbits are similar but time-shifted. In Fig. 9 we show the cross-correlation coefficient

$$r = \frac{\sum (x_1(t) - \bar{x}_1)(x_2(t-\tau) - \bar{x}_2)}{\|x_1(t) - \bar{x}_1\| \, \|x_2(t) - \bar{x}_2\|}$$

where $\bar{x}_j$is the mean value of the amplitude along the trajectory. The coefficient r is bounded in the range $(-1, 1)$, where -1 and 1 indicate in-phase and anti-phase relation and 0 corresponds to lack of correlation. As it is easy to see that the cross-correlation coefficient stays high for periodic, quasiperiodic, and chaotic cases and decays to zero in the case of the hyperchaotic attractor.

The electrical experiment agrees with our numerical findings. In Figs. 8(a-c) experimental time traces from the array of electrical circuits (Fig. 5) are presented for all three cases: periodic (Fig. 8(a)), quasi-periodic (Fig. 8(b)) and chaotic (Fig. 8(c)) rotating waves. It is

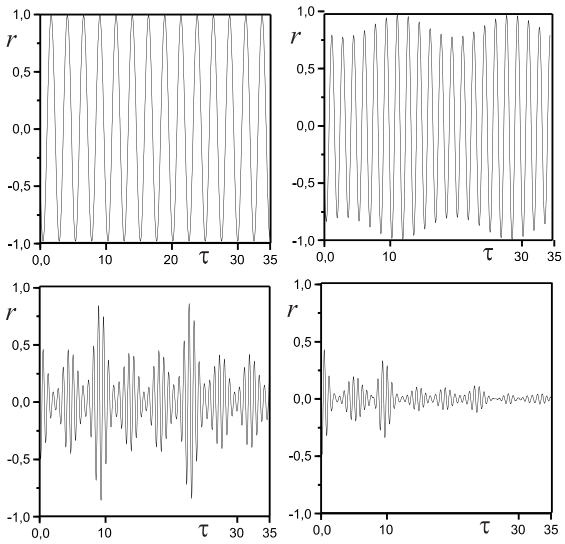

Figure 9: Typical behavior of correlation coefficient for four types of attractors. Periodic ($k = 0.3$), quasiperiodic ($k = 0.5$), chaotic ($k = 1.85$), and hyperchaotic ($k = 2.1$).

easy to observe that the time-shift symmetry between time traces of subsequent oscillators approximately persists in all three cases mentioned above.

V. LARGE NETWORK

The number of nodes plays an important role for the development of complex behavior in the networks of coupled oscillators, see e.g. [52]. In this section, we investigate the dynamics of a large network of unidirectionally coupled Duffing oscillators (2) with $N = 400$. The choice of N is motivated from one side by numerical limitations (path-following of a large system) and from another side by the fact that this is about the value where some important spatio-temporal features like Eckhaus phenomenon become visible. In Fig. 10 we show the bifurcation diagram versus coupling coefficient k. The transition to chaotic behavior takes place for a much lower value of the coupling coefficient ($k = 0.1435$) than in the case of three coupled oscillators, but also one can observe the coexistence of several stable periodic solutions, and the coexistence of stable periodic solutions and chaos (see Fig. 11).

As it was mentioned in Sec. III, in a ring of $N = 400$ coupled systems one can observe $(N-1)/2$ Hopf bifurcations of the symmetric equilibrium. Each bifurcation leads to the appearance of a branch of *periodic solutions* (PS) and most of the branches are unstable. The increase of the number of unstable PS indicates already that one should expect here more complex dynamics as the coupling parameter increases. The Hopf curve, on which PS

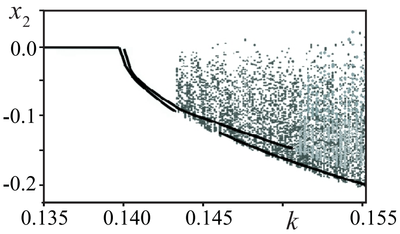

Figure 10: Bifurcation diagram for 400 unidirectionally coupled Duffing oscillators versus coupling coefficient k. Parameters of the system: $a = 0.1$, $d = 0.3$.

appear, can be obtained from the condition

$$i\omega = -\frac{d}{2} + \sqrt{\left(\frac{d}{2}\right)^2 - a - k\left(1 - e^{i\varphi}\right)}, \qquad (14)$$

where the real part of eigenvalues (13) vanishes at Hopf bifurcation. Eq. (14) can be solved with respect to the coupling parameter k and the Hopf frequency ω

$$\begin{aligned} k(\varphi) &= \tfrac{\omega(\varphi)d}{\sin\varphi}, \\ \omega(\varphi) &= \tfrac{d\alpha(\varphi)}{2} + \sqrt{\left(\tfrac{d\alpha(\varphi)}{2}\right)^2 + a}, \end{aligned} \qquad (15)$$

where $\alpha(\varphi) = (1 - \cos\varphi)/\sin\varphi$ and $\varphi \in (0, 2\pi)$ is the parameter along the Hopf curve. We take into account only positive solutions with $k(\varphi) \geq 0$. The Hopf curve is shown in Fig. 11 as blue line (color online), from which the branches of PS emerge. Note that the period of the emerging PS on the Hopf curve is $T(\varphi) = 2\pi/\omega(\varphi)$.

In Fig. 11(a) we plot the period T along the branches of PS versus coupling coefficient k. All shown solutions are rotating waves. The branches have been calculated numerically by path following method using the software package AUTO [53]. Due to numerical limitations we calculate only the twelve PS branches closest to the stable region. In Fig. 11(d) the Hopf bifurcation curve is shown in a wide range of k, while in other plots (Fig. 11(a,c)) only a small part is shown. Stable and unstable PS along the branches are shown by black and gray lines respectively. In Fig. 11(c) we show an enlargement of the left part of Fig. 11(a). In addition to the numerically computed branches of PS (grey lines), we show schematically also other branches, which appear from the Hopf bifurcation of the symmetric equilibrium (gray dashed lines). One can observe here the occurrence of the Eckhaus scenario [19, 24, 25], i.e. the emergence of a region of stable PS that covers a certain range of frequencies and spatial wave numbers in the neighborhood of the primary stable branch, emerging from the primary Hopf bifurcation. Except for the primary branch, the PS branches emerge unstable at the Hopf bifurcation. Then the branches closest to the primary branch become stable in a cascade of Neimark-Sacker bifurcations. Note that here, the stability region is rather narrow and some branches are leaving the stability region after passing through a further

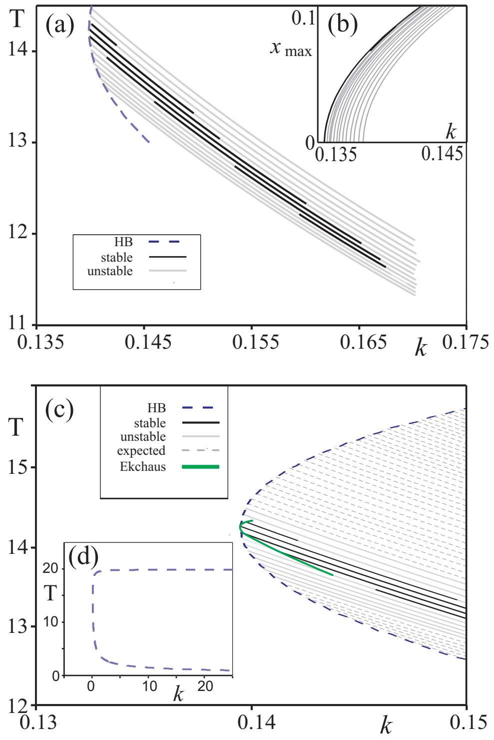

Figure 11: Period T (a,c) and maximum amplitude of oscillations x_{max} (b) along branches of periodic solutions for 400 unidirectionally coupled Duffing oscillators versus coupling coefficient k. The zoom and extension of (a) is shown in (c). The Hopf bifurcation curve calculated from Eq. (15) is shown in (d). Stable periodic solution - black bold line, unstable periodic solution - gray lines; Hopf curve - bold blue dashed line, Eckhaus stability boundary - bold green line. Parameters of the system are $d = 0.3$ and $a = 0.1$.

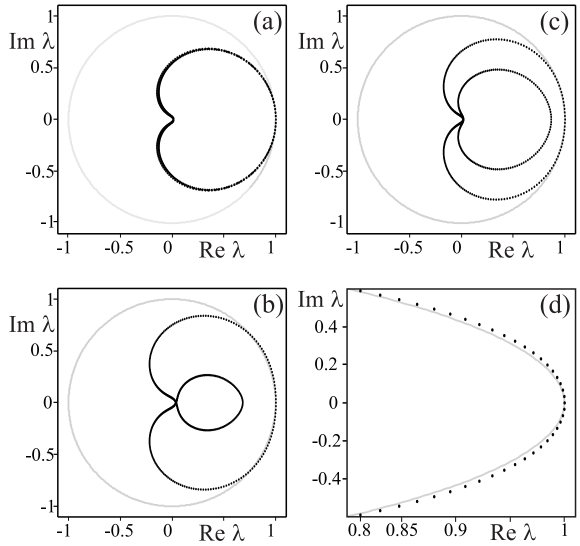

Figure 12: Floquet multipliers (black dots) of the PS on the first branch (see fig. 11(a)) for coupling coefficient $k = 0.140$ (a), $k = 0.148$ (b), $k = 0.171$ (c,d). The unit circle is shown in gray. The other parameters are $d = 0.3$ and $a = 0.1$.

Neimark-Saker bifurcation. The Eckhaus curve which encloses the stable region is shown in green and does not depend on N. Fig. 11(b) shows the same PS branches as in Fig. 11(a,c) displaying the maximum amplitude of oscillation x_{max} versus the coupling coefficient k[55].

An important property of the Eckhaus stability region is its independence of the number of oscillators [25] in the network. With an increasing number of oscillators, the PS branches become more dense, thus filling more and more densely the Eckhaus stability region. In our example of Duffing oscillators this region is rather small and therefore multiple coexistence can be observed only for large N.

Let us investigate now in more detail the stability along the first branch of PS. Just after the supercritical Hopf bifurcation, the branch is stable until it escapes the Eckhaus region with increasing of k. The stability of a PS is determined by the spectrum of Floquet multipliers, see Fig. 12. The PS is stable when all Floquet multipliers are inside the unit circle, otherwise PS is unstable. As in the case of equilibria, one can observe that the spectrum is again aligned along curves of asymptotic continuous Floquet spectrum. The main bifurcations in this case will be Neimark-Saker bifurcations, i.e. when a complex conjugate pair of Floquet multipliers ($\mathrm{Im}\,(\lambda) \neq 0$) is crossing the unit circle. Examples of stable spectra are shown in Fig. 12(a,b) for $k = 0.14$ and $k = 0.148$, respectively. The unstable spectrum for $k = 0.171$ is shown in Fig. 12(c) and its enlargement in Fig. 12(d). One can observe that for $k = 0.171$ the corresponding PS has already multiple unstable dimensions.

In Fig. 13 we show some spatio-temporal plots. The oscillator number is shown along the horizontal axis and the time along the horizontal axis. The amplitude of oscillators $x_j(t)$ is shown using a color gradient. For better visibility we restricted the space to $N = 200$ oscillators. In Fig. 13(a) one observes a pattern corresponding to a stable periodic rotating wave. The corresponding initial conditions are taken from the primary branch of PS with $k = 0.148$. With increasing k, the PS escapes the Eckhaus stability region and becomes unstable. The solution shows now the irregular pattern given in Fig. 13(b) for $k = 0.171$. Although all the rotating waves are already unstable, an intermittent periodic structure still exists locally in space and time. The existence of such structures indicates that the unstable rotating waves become a part of a new chaotic attractor after destabilization. As a result, the system visits intermittently and locally in space such unstable PS during its evolution along the chaotic attractor [54]. This phenomenon can be seen in more detail in Fig. 14 where we show two cross-sections of Fig. 13(b). The first one shows the time evolution of one fixed oscillator (Fig. 14(a,b)). The second shows the amplitudes of all oscillators for some fixed time moment (Fig. 14(c,d)). We plot the hyperchaotic trajectory (black) and the unstable PS from the primary branch (grey). The black dots in Figs. 14(c,d) indicate the po-

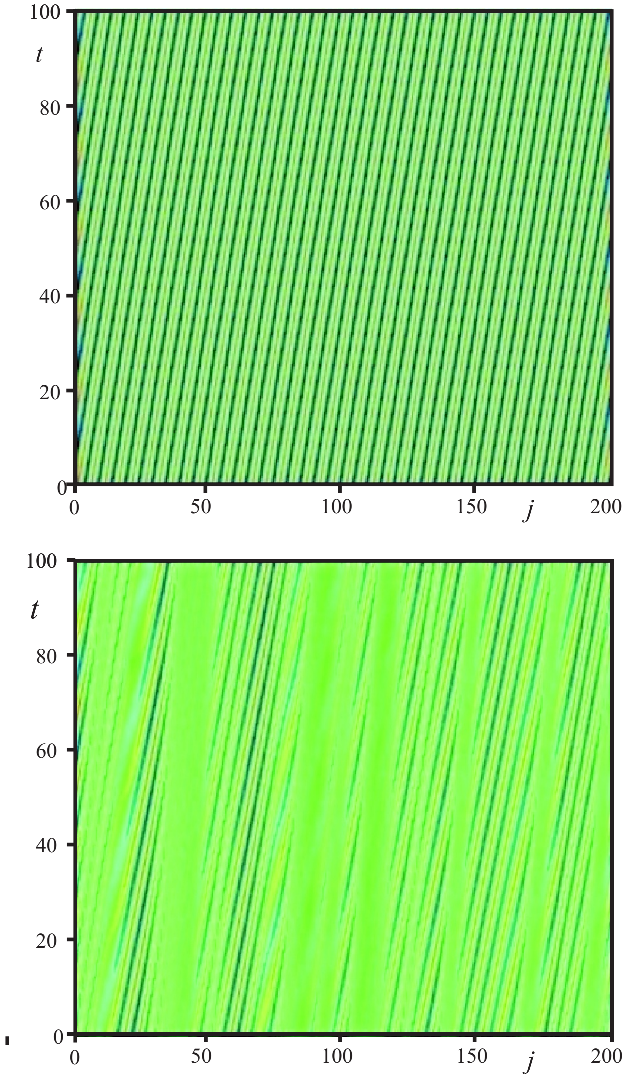

Figure 13: Spatio-temporal plots for 400 coupled Duffing oscillators. Number of oscillators versus time. Oscillation amplitude is shown by a color gradient. Stable periodic pattern for $k = 0.148$ (a) and chaotic dynamics for $k = 0.171$ (b). The space is restricted to $1 \leq j \leq 200$.

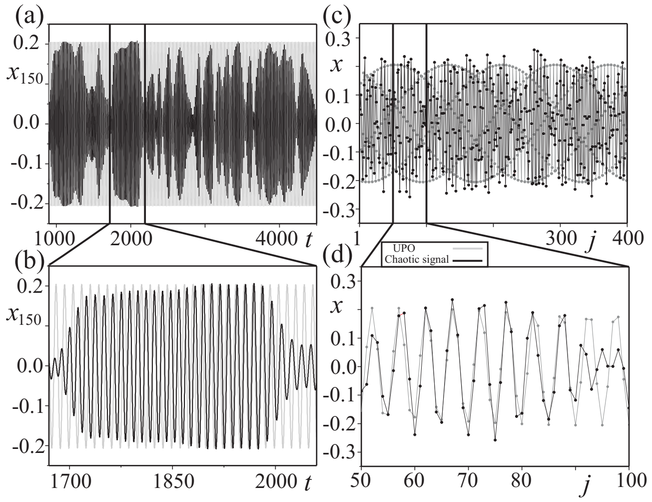

Figure 14: Cross sections of spatio-temporal plot (Fig. 13) in time (a,b) and in space (c,d). Chaotic time evolution (black line) and irregular spatial pattern (black dots) follow locally the unstable PS on the primary branch (grey); $k = 0.171$.

sitions of single oscillators. Fig. 14(a) shows that the chaotic trajectory frequently comes close to the unstable PS (see also enlargement in Fig. 14(b)), where the amplitude and the period of the chaotic trajectory and PS are close. The same scenario can be observed in the second cross-section in Fig. 14(c,d). In Fig 14(d) it is easy to see the good local correlation between the spatial profile of the chaotic orbit and of the unstable PS.

VI. CONCLUSION

We studied the appearance of complex dynamics in a ring of unidirectionally coupled autonomous Duffing oscillators. Although the individual uncoupled system has only trivial dynamics as a globally stable equilibrium, the system shows with increasing coupling strength a transition to periodic, quasiperiodic and chaotic behavior. The symmetry in the coupling structure leads to the appearance of rotating waves with a fixed phase relation between neighboring oscillators, which can be traced also within the region of quasiperiodic and chaotic behavior and manifests in the form of chaotic rotating waves. If the number of oscillators in the ring is large, the system shows additional interesting phenomena. After destabilization we observed the coexistence of multiple stable periodic solutions in a band of frequencies and wave numbers close to the primary branch of periodic solutions, that can be interpreted in terms of the well known Eckhaus scenario. We identified the symmetric unstable periodic orbits, which are in the skeletons of the chaotic attractor and discuss their role in the development of spatio-temporal structures. Some of our theoretical results have been confirmed in an experiment with three coupled Duffing oscillators. We were able to observe experimentally periodic, quasiperiodic, chaotic, and hyperchaotic signals, as well as chaotic rotating waves.

Acknowledgments

P.P., S.Y. and M.W. acknowledge the support of DFG Research Center Matheon “Mathematics for key technologies”. P.P., S.Y., M.W., A.S. and T.K. acknowledge the support of DAAD cooperation under Project No. D0700430, and Department of International Co-operation of Poland under Project DWM/ N97/DAAD/2008. P.M. is a scholarship holder of project entitled "Innovative education ..." supported by European Social Fund under Project No.

11/U/39/I/SD/2008.

[1] S. H. Strogatz, Nature **410**, 268 (2001).
[2] R. Zillmer, R. Livi, A. Politi, and A. Torcini, Phys. Rev. E **74**, 036203 (2006).
[3] E. Mosekilde, Y. Maistrenko, and D. Postnov, *Chaotic Synchronization. Application to Living Systems.* (World Scientific, 2002).
[4] A. Pikovsky, M. Rosenblum, and J. Kurths, *Synchronization. A Universal Concept in Nonlinear Sciences* (Cambridge University Press, 2001).
[5] O. Rossler, Phys. Lett. A **57**, 397 (1976).
[6] G. Baier and M. Klein, *A Chaotic Hierarchy* (World Scientific, Singapore, 1991).
[7] J. Peinke, J. Parisi, O. E. Rossler, and R. Stoop, *Encounter with Chaos* (Springer, Berlin, 1992).
[8] T. Kapitaniak, L. Chua, and G.-Q. Zhong, IEEE Transactions on Circuits and Systems I: Fundamental Theory and Applications **41**, 499 (1994).
[9] T. Kapitaniak and L. O. Chua (1993), URL `http://www.eecs.berkeley.edu/Pubs/TechRpts/1993/2462.html`.
[10] T. Kapitaniak and W. H. Steeb, Physics Letters A **152**, 33 (1991), ISSN 0375-9601, URL `http://www.sciencedirect.com/science/article/B6TVM-46SNMD3-14H/2/4a6871c457e4facf16a0d3425506cdb6`.
[11] T. Kapitaniak, Phys. Rev. E **47**, R2975 (1993).
[12] M. A. Harrison and Y.-C. Lai, Phys. Rev. E **59**, R3799 (1999).
[13] Y.-C. Lai, Phys. Rev. E **59**, R3807 (1999).
[14] S. Yanchuk and T. Kapitaniak, Phys. Lett. A **290**, 139 (2001).
[15] T. Kapitaniak, Y. Maistrenko, and S. Popovich, Phys. Rev. E **62**, 1972 (2000).
[16] M. A. Matías and J. Güémez, Phys. Rev. Lett. **81**, 4124 (1998).
[17] X. L. Deng and H. B. Huang, Phys. Rev. E **65**, 055202 (2002).
[18] I. P. Marino, V. Pérez-Mu nuzuri, V. Pérez-Villar, E. Sánchez, and M. A. Matías, Phys. D **128**, 224 (1999), ISSN 0167-2789.
[19] W. Eckhaus, *Studies in Non-Linear Stability Theory* (Springer Tracts in Natural Philosophy, 1965).
[20] K. Tsiveriotis and R. A. Brown, Phys. Rev. Lett. **63**, 2048 (1989).
[21] L. S. Tuckerman and D. Barkley, Physica D **46**, 57 (1990).
[22] L. Tuckerman and D. Barkley, Phys. Rev. Lett. **67**, 1051 (1991).
[23] N. Mukolobwiez, A. Chiffaudel, and F. Daviaud, Phys. Rev. Lett. **80**, 4661 (1998).
[24] M. Wolfrum and S. Yanchuk, Phys. Rev. Lett. **96**, 220201 (2006).
[25] S. Yanchuk and M. Wolfrum, Phys. Rev. E **77**, 026212 (pages 7) (2008), URL `http://link.aps.org/abstract/PRE/v77/e026212`.
[26] A. B. Rovinsky and M. Menzinger, Phys. Rev. Lett. **69**, 1193 (1992).
[27] V. Z. Yakhnin, A. B. Rovinsky, and M. Menzinger, The Journal of Physical Chemistry **98**, 2116 (1994), http://pubs.acs.org/doi/pdf/10.1021/j100059a023, URL `http://pubs.acs.org/doi/abs/10.1021/j100059a023`.
[28] L. Schimansky-Geier, M. Mieth, H. Rosé, and H. Malchow, Physics Letters A **207**, 140 (1995), ISSN 0375-9601, URL `http://www.sciencedirect.com/science/article/B6TVM-3YCF3BX-3P/2/cfbca45890a2d78f7c14f4552b0afdaa`.
[29] L. M. Pecora and T. L. Carroll, Phys. Rev. Lett. **80**, 2109 (1998).
[30] A. Wolf, J. Swift, H. Swinney, and J. Vastano, Physica D **16**, 285 (1985).
[31] A. Wolf, *Quantifying chaos with Lyapunov exponents*, Chaos (V. Holden eds) (Manchester University Press, Manchester, 1986).
[32] P. Perlikowski, B. Jagiello, A. Stefanski, and T. Kapitaniak, Physical Review E (Statistical, Nonlinear, and Soft Matter Physics) **78**, 017203 (pages 4) (2008), URL `http://link.aps.org/abstract/PRE/v78/e017203`.
[33] B. Nana and P. Woafo, Phys. Rev. E **74**, 046213 (2006).
[34] P. Perlikowski, A. Stefanski, and T. Kapitaniak, Physical Review E **77** (2008).
[35] *Low Cost Analog Multiplier*, Analog Devices, Inc. (2002).
[36] F. N. H. Robinson, IMA Journal of Applied Mathematics **42**, 177 (1989).
[37] M. Golubitsky and D. G. Schaeffer, *Singularities and Groups in Bifurcation Theory. Volume I*, vol. 51 of *Applied Mathematical Sciences* (Springer-Verlag, 1985).
[38] M. Golubitsky, I. Stewart, and D. G. Schaeffer, *Singularities and Groups in Bifurcation Theory. Volume II*, vol. 69 of *Applied Mathematical Sciences* (Springer-Verlag, 1988).
[39] M. Golubitsky and I. Stewart, in *Equadiff 2003: Proceedings of the International Conference on Differential Equations*, edited by F. Dumortier, H. Broer, J. Mawhin, A. Vanderbauwhede, and S. V. Lunel (World Scientific, 2005), pp. 13–24.
[40] L. M. Pecora and T. L. Carroll, Phys. Rev. Lett. **64**, 821 (1990).
[41] M. G. Rosenblum, A. S. Pikovsky, and J. Kurths, Phys. Rev. Lett. **76**, 1804 (1996).
[42] A. Pikovsky, M. Rosenblum, and J. Kurths, IEEE Trans. Circuits Syst **44(10)**, 874 (1997).
[43] G. V. der Sande, M. C. Soriano, I. Fischer, , and C. R. Mirasso, to appear in PRL 2008.
[44] N. F. Rulkov, M. M. Sushchik, L. S. Tsimring, and H. D. I. Abarbanel, Phys. Rev. E **51**, 980 (1995).
[45] K. Kaneko, Physica D: Nonlinear Phenomena **37**, 60 (1989).
[46] V. N. Belykh and E. Mosekilde, Phys. Rev. E **54**, 3196 (1996).
[47] V. N. Belykh, I. V. Belykh, and K. V. Nelvidin, Math. Comput. Simul. **58**, 477 (2002), ISSN 0378-4754.
[48] T. Pereira, M. S. Baptista, and J. Kurths, Physical Review E (Statistical, Nonlinear, and Soft Matter Physics) **75**, 026216 (pages 12) (2007).
[49] G. Hu, Y. Zhang, H. A. Cerdeira, and S. Chen, Phys. Rev. Lett. **85**, 3377 (2000).
[50] E. Sánchez and M. A. Matías, Phys. Rev. E **57**, 6184

(1998).
[51] Y. Zhang, G. Hu, and H. A. Cerdeira, Phys. Rev. E **64**, 037203 (2001).
[52] S. H. Strogatz, D. M. Abrams, A. McRobie, B. Eckhardt, and E. Ott, Nature **438**, 43 (2005), ISSN 0028-0836, URL `http://dx.doi.org/10.1038/43843a`.
[53] E. J. Doedel, *AUTO-07P: Continuation and bifurcation software for ordinary differential equations*, Concordia University, Montreal, Canada (2006), URL `http://sourceforge.net/projects/auto2000`.
[54] E. Ott, *Chaos in Dynamical Systems (Second edition)* (Cambridge University press, 2002).
[55] All considered PSs have the structure of rotating waves, thus the amplitudes of all oscillators are the same.